Accepted Manuscript

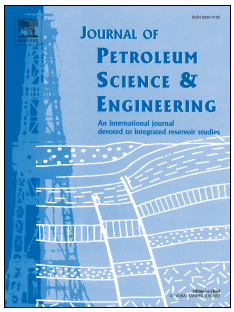

Detectability of smart proppants traced with gadolinium and samarium in the Vaca Muerta formation

María S. Herrera, Alberto Ortiz, Damián Hryb, Nicolás M. Rendtorff

PII: S0920-4105(19)30401-2

DOI: https://doi.org/10.1016/j.petrol.2019.04.064

Reference: PETROL 6003

To appear in: *Journal of Petroleum Science and Engineering*

Received Date: 27 August 2018

Revised Date: 8 April 2019

Accepted Date: 18 April 2019

Please cite this article as: Herrera, Marí.S., Ortiz, A., Hryb, Damiá., Rendtorff, Nicolá.M., Detectability of smart proppants traced with gadolinium and samarium in the Vaca Muerta formation, *Journal of Petroleum Science and Engineering* (2019), doi: https://doi.org/10.1016/j.petrol.2019.04.064.

Highlights:

- The use of traceable samarium-based proppants was confirmed by Monte Carlo simulations.
- Realistic borehole-formation-tool models with and without proppants were studied.
- A minimum samarium oxide concentration of 1.25 % wt. is needed to be detected.

Detectability of smart proppants traced with gadolinium and samarium in the Vaca Muerta formation

María S. Herrera[a,*], Alberto Ortiz[b], Damián Hryb[b], Nicolás M. Rendtorff[c,d]

[a] *YPF Tecnología S. A., (Y-TEC - CONICET), Av. del Petróleo s/n, e 129 y 143 (1923), Berisso, Argentina*
[b] *YPF S. A., Macacha Güemes 515 (1425), Buenos Aires, Argentina*
[c] *Dpto. De Química, Facultad de Ciencias Exactas, Universidad Nacional de La Plata, UNLP, 47 y 115 s/n, La Plata, Argentina*
[d] *Centro de Tecnología de Recursos Minerales y Cerámica (CETMIC - CIC-CONICET-CCT La Plata), Cno. Centenario y 506 s/n, C.C.49 (B1897ZCA), M. B. Gonnet, Argentina*

Abstract

The use of smart proppants traced with gadolinium and samarium was evaluated in a realistic model by Monte Carlo simulations.

The addition of compounds with high thermal neutron capture cross section, such as gadolinium oxide (Gd_2O_3) and samarium oxide (Sm_2O_3) into ceramic proppants, makes them detectable after placement in induced fractures.

Proppants traced with different oxide concentrations were studied in a generic borehole-formation-tool configuration, modeled with MCNP. The Vaca Muerta formation model was constructed based on measured geochemical data. A theoretical formation of water-saturated limestone with 20 % porosity was also used as a reference case of study. The minimum concentration of gadolinium and samarium oxides needed, in order to make them detectable by logging tools, was determined. In the case of gadolinium, results are in agreement with previous reported values for Gd_2O_3 addition of about 0.4 % by weight of proppant. In the case of samarium, a minimum concentration of 1.25 % by weight of Sm_2O_3 addition could be detected in both Limestone and Vaca Muerta formations.

Keywords: Vaca Muerta formation, Traceable proppant, Samarium oxide,

*Corresponding author
Email address: m.silvia.herrera@ypftecnologia.com (María S. Herrera)

Gadolinium oxide, Thermal neutron capture cross section, MCNP
2010 MSC: 82D75, 65C05

1. Introduction

The Vaca Muerta formation is the most relevant reservoir for unconventional hydrocarbons production in Argentina (Ortiz et al., 2016) and it is ranked second and fourth in the world for shale oil and shale gas, respectively (EIA, 2013). From a total of 800 trillion cubic feet of estimated resources, around 27 % are assigned to Vaca Muerta (Stinco and Barredo, 2014). The reservoir, located in the Neuquén basin, has been extensively described in (Suarez et al., 2015; Stinco and Barredo, 2014; Sagasti et al., 2014; Suarez et al., 2013) and references therein. This formation is represented by organic shales and marls with thickness varying from 25 to 450 m (Ortiz et al., 2016; Stinco and Barredo, 2014). It comprises a wide variety of lithologies, composed primarily by intercalations of organic-rich calcareous shales, marls, and micritic limestones (Sagasti et al., 2014). Vaca Muerta formation shows different facies related to depositional characteristics and its position within the basin, with total organic concentration (TOC) variations from almost 15 % at the base down to less than 2 % to the top. Values of porosity range from 9 to 13 porosity units (Ortiz et al., 2016). Limestone layers, calcite veins and calcified and non-calcified volcanoclastic beds are also present (Ortiz et al., 2016).

The process used to produce shale oil in Vaca Muerta, is hydraulic fracturing. It mainly consists of the injection of high pressure water and proppant particles in the wells, to stimulate the formation of very low permeability. The results of which is an artificial fracture network where the fluids move. The proppant material is used to keep these induced fractures open, preventing blockage of fluid drainage. Proppants used in the fracturing process include natural sands, resin coated sands and ceramic proppants (Liang et al., 2016). Ceramic proppants belong to the $Al_2O_3{-}SiO_2$ system and are manufactured from kaolin and/or bauxitic clays (Mocciaro et al., 2018; Liang et al., 2016; Smith et al., 2012).

Compared to silica sands, ceramic proppants are stronger and more crush resistant, especially where closure stresses exceed 8,000 to 10,000 psi (Liang et al., 2016). In Vaca Muerta, each hydraulic stimulation uses aproximmately 230 tons of proppants per fracture, of which 23 tons are ceramics.

Hydraulic fracturing is effective in the production of hydrocarbons, however, it is a non-specific technique, since the location and growth of the fractures are unknown. As a result, important uncertainties occur in the analysis of the productivity of the wells.

Determine proppant placement and fracture geometry after a fracturing job can add significant value to stimulation treatments and completetion processes. Propped fracture height measurements can be used to calibrate geomechanical models, improving the accuracy of the stimulated reservoir volume (SRV). Moreover, measurement of the proppant location allows to verify whether all zones were stimulated as planned, which has direct impact on reservoir recovery.

Methods to identify proppants in induced fractures have been proposed in patents US8234072 and US8234072 (Smith et al., 2012; Smith and Duenckel, 2014). These methods require the incorporation of a traceable compound with high thermal neutron capture cross section, into the proppant grain.

Elements such as gadolinium, samarium, iridium, cadmium and boron, have high avidity for absorbing slow or "thermal" neutrons (energy range < 0.5 eV). The incorporation of such elements into proppants grains would increase their macroscopic thermal neutron capture cross section and makes them detectable by conventional nuclear logging tools near wellbore.

In petrophysics, it is common to use the macroscopic thermal neutron capture cross section (Σ) as a bulk property for neutron interactions with materials. This parameter, also referred to as sigma, is defined as the product of the microscopic capture cross sections per atom of the individual formation nuclei (i) and the number of atoms per cubic centimeter N (Ellis et al., 2003):

$$\Sigma_i = N\sigma_i = \frac{N_{av}\rho}{A}\sigma_i\,, \tag{1}$$

where, N_{av} is the Avogadro's number, ρ is the density (in g cm^{-3}), and A is the atomic weight of the isotope. Note that Σ has dimension of cm^{-1}, however, the so-called capture units (c.u.) are preferably used in petrophysics to avoid using small numbers, multiplying by 1,000 times Σ.

In other words, the addition of elements such as gadolinium (49,700 b) and samarium (5,922 b) increases the macroscopic thermal neutron capture cross section of the proppant and makes it detectable after placement in the fracture. This is mainly achieved by measuring the suppression of the thermal neutron flux recorded in the post-frac log, or computing the gadolinium yield through gamma spectroscopy. After-fracture signals are often compared to the corresponding before-fracture signals, showing the presence (or absence) of the traceable material.

Up to date there is only one treaceble proppant (ceramic) available in the market which uses gadolinium oxide. The technology has been successfully employed over 200 vertical wells in field operations (Duenckel et al., 2011; Torres et al., 2012; Smith et al., 2013; Han et al., 2014; Saldungaray et al., 2014; Duenckel et al., 2014; Liu et al., 2015; Ortiz et al., 2016; Zhang and Smith, 2017; Zhang et al., 2018; Oliveria Neto and Yakovlev, 2017). Recently, a feasibility study of locating and evaluating hydraulic fractures in horizontal wells using Gd-based ceramic proppants have been published (Zhang et al., 2018). The field test, with a total of 50 perforation clusters and eight stages, demostrated that traceable proppants can be detected with tracer signals clearly observed in all stages.

The ceramic behavior of gadolinium oxide and samarium oxide-ball clay mixtures, for high macroscopic neutron capture cross section proppants design, has been previously reported by our group (Herrera et al., 2019; Hernández et al., 2017). It was concluded that the incorporation of those rare earth oxides to a possible formulation of a kaolinitic clay-based ceramic proppant would not imply significant changes in the processing route. The optimum oxide concentration

in the proppant depends on several factors, including the detection system, the mechanical properties of the the traceable and its cost.

In the present paper, Monte Carlo simulations were used for the assessment of using both gadolinium and samarium oxides traceable ceramic proppants in the Vaca Muerta formation. The minimum concentration of gadolinium and samarium oxides needed, in order to make them detectable in the formation were determined. To this end, the general-purpose Monte Carlo N-Particle radiation transport code (MCNP) was used. MCNP is a radiation transport code that can be used for neutron, photon and electron transport calculations in 3-D configurations (X-5 Monte Carlo Team, 2008). Since complex geometries can be modeled, the program is widely used in the petroleum industry and well logging problems (Wang et al., 2017; van der Hoeven et al., 2017; Ortega et al., 2014; Mendoza et al., 2007; Wielopolski et al., 2005; Forster et al., 1990; Preeg and Scott, 1986).

The proppant materials were evaluated in a borehole-formation-tool configuration. In particular, a theoretical fresh water-saturated 20 p.u. limestone formation was modeled as a reference case of study. Then, a complex matrix based on measured geochemical results from the Vaca Muerta formation, was used. This case allowed to evaluate the traceable smart proppants in real downhole conditions, with presence of strongly absorbing elements such as gadolinium, samarium, boron and others.

2. Methodology and computational model

A computational model of a generic borehole-formation-tool configuration was built using the MCNP code, version 5 (X-5 Monte Carlo Team, 2008). The configuration consists of a cube formation with a bi-wing fracture, a cemented and cased hole and a generic nuclear logging tool.

The tool includes a pulsed neutron source and three thermal neutron detectors. Proportional counters filled with helium (^{3}He) gas are the gold standard for thermal neutron detection (Amaro et al., 2017), and they are commonly used

in the petroleum industry.

Thermal neutron detection is based on the $^3He + n \rightarrow {}^3H + p + 765$ keV nuclear reaction. Neutrons interact with ^3He gas through the (n,p) reaction. The energy of the reaction (Q = 765 keV) is carried away as kinetic energy of the products, proton (p) and tritium (^3H), producing a detectable charge with an output pulse proportional to 765 keV.

In real logs, the total neutron count rate (neutrons per second) is measured by the neutron tool. In this work, the (n,p) reaction rate (reactions per second) is reported. In the ideal case, these two quantities are equal.

The (n,p) reaction rate can be computed in MCNP, using appropriate tally multipliers (FM cards). Thus, the (n,p) reaction rate is determined in the detectors using the cell flux tally (F4) and an energy bin from 0 to 0.4 eV.

A straightforward variance reduction technique of importance sampling was used in the simulations. Typical runs involved 10^9 particles yielding relative statistical errors lower than 0.5 % for each detector.

In MCNP, the problem geometry is specified using cells containing user-defined materials. A material is a combination of elements (or isotopes). The fraction by mass or weight is specified for each component. Both, the elemental composition and the bulk density are essential information for MCNP calculations. In the next sections, the geometry and elemental composition of the borehole-formation-tool configuration and the traceable proppant are described.

2.1. Borehole and nuclear logging tool

The borehole is a cemented (portland, 1.92 g cm^{-3}) and cased hole of 8 inches in diameter. Carbon steel (7.86 g cm^{-3}) was assumed for the tubing. The borehole fluid was fresh water (1.0 g cm^{-3}). The tool is located inside the borehole, 1.8 cm from the center of the borehole to the right against the casing (no tool standoff), as it is shown in Figure 1.

The tool model was based on scattered data found in the literature, since nuclear logging tools designs are owned by service companies. It consists of a pulse neutron source, two shielding blocks and three thermal neutron detectors. Fast

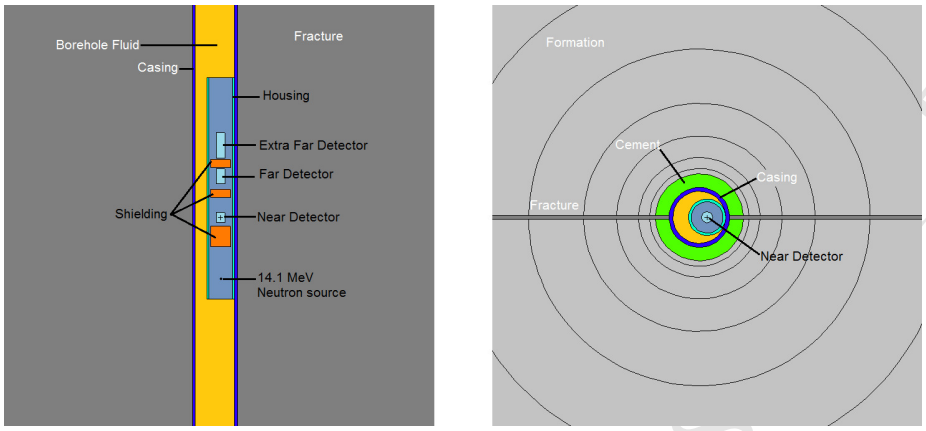

Figure 1: Cross section view of the generic borehole-formation-tool configuration and the down hole bi-wing fracture geometry, modeled in MCNP5. Colors show the different components, labelled in the figure.

neutrons are produced by a compact neutron generator based on the deuterium-tritium fusion reaction, $^{2}\mathrm{H} + {}^{3}\mathrm{H} \rightarrow {}^{4}\mathrm{He} + \mathrm{n} + 17.59$ MeV. The Q-value for this reaction is 17.59 MeV and is shared by a neutron and an alpha particle (^{4}He). The neutron generator is operated in a sealed-tube in which deuterium (^{2}H) ions are accelerated to impinge on a target of tritium (^{3}H) where the nuclear fusion occurs.

The components are located inside the tool wall of stainless steel (7.8 g cm^{-3}). The tool body length is 43 inches with an outer radius of 1 11/16 in (Mendoza et al., 2007; Maucec and Spanier, 2000). The detectors are named: near, far and extra far detectors (ND, FD, XFD, respectively), and are filled with helium-3 gas at 4 atm (Mendoza et al., 2007; Maucec and Spanier, 2000; Serov et al., 1998).

The neutron source is located 20 cm from the bottom of the tool. Monoenergetic neutrons burst of 30 μs and 14.1 MeV are emitted in all directions. The intensity of the source was set at 10^{8} neutrons per second.

A neutron shielding material of boron carbide (B_4C, 2.52 g cm^{-3}) was employed. The shielding avoids neutrons pass directly from the neutron source to the detectors.

Distances from the neutron source to the center of the detectors are 8, 16 and 22 inches, for ND, FD and XFD, respectively. Typical detector heights of 2, 3 and 8 in. were used. The diameter of all detectors was set at 1 inches (Mendoza et al., 2007; Maucec and Spanier, 2000).

2.2. Formation model

The formation was modeled as a cube of 350 cm side with a bi-wing fracture. Figure 1 shows the proppant in the fracture in dark gray color. The proppant is replaced in the fracture and it is assumed to be distributed homogenously. Two different fracture widths of 1 and 10 mm were used in the formation model. Two homogenized formations of different composition and porosity were modeled. First, a theoretical water-saturated limestone of 20 % porosity was used as a reference case of study. Second, a complex matrix formation based on measured geochemical results from the Vaca Muerta (VM) formation in the Neuquén basin of Argentina, was used as a real case. This is the first time that the elemental composition of VM is described for MCNP calculations.

The isotopic mixture rather than the simpler elemental composition of both formations was computed using the MatMCNP program (Version 3.0) (Russell DePriest and Saavedra, 2014), distributed by Sandia National Laboratories. When available, neutron thermal scattering data (S(α, β)) was used through appropriate reaction type numbers (MT cards).

2.2.1. Limestone formation composition

The theoretical formation consists of limestone of 20 % porosity saturated with fresh water. The elemental composition of limestone was taken from (McConn et al., 2011). Based on the densities of solid limestone (2.61 g cm^{-3} (McConn et al., 2011)) and fresh water, a formation fluid density of 2.29 g cm^{-3} was assumed in the simulations. In Table 1 the element weight fraction of the matrix is shown.

Table 1: Limestone 20 p.u. water-filled matrix elemental composition used in the simulations. Weight fractions were computed assuming a bulk density of 2.29 g cm^{-3}. Σ = 9.3 c.u., calculated using 1.

Element	Weight fraction (% wt.)
Oxygen	52.6166
Calcium	28.3641
Carbon	10.551
Sodium	4.4726
Silicon	2.2644
Hydrogen	0.8967
Aluminum	0.3944
Iron	0.3258
Titanium	0.0337
Lead	0.0312
Potassium	0.0309
Sulfur	0.0185

2.2.2. Vaca Muerta formation composition

The Vaca Muerta formation elements were determined from measured geochemical results. Major oxides concentrations, shown in Table 2, were measured by X-Ray Fluorescence (XRF). A multi-element analysis under Inductively Coupled Plasma Mass Spectrometry (ICP-MS) allowed to determine the concentration of 30 elements, including rare earth elements such as gadolinium and samarium. Coulometry method Leco was used to determine the carbon and sulfur content. Based on these measurements, the VM matrix was constructed. Table 3 shows the VM 5 p.u. water-filled matrix elemental composition used in the simulations. Weight fractions were computed assuming a bulk density of 2.4 g/cm^3.

Unlike limestone, the elements present in the VM matrix includes strongly absorbing elements such as gadolinium (3 ppm), samarium (3 ppm) and boron (71

Table 2: Mean values of the major oxides present in the Vaca Muerta formation measured by X-Ray Fluorescence.

Oxide	Weight fraction (% wt.)
SiO_2	37.38
CaO	21.15
Al_2O_3	8.46
Fe_2O_3	2.47
K_2O	1.82
MgO	1.66
Na_2O	1.48
P_2O_5	0.42
TiO_2	0.30
V_2O_5	0.04
MnO	0.06

ppm).

As it is shown in Table 3, high concentrations of barium (3,000 ppm) and strontium (10,000 ppm) are present in the formation. Values exceeding 10,000 ppm were measured by GO_XRF76V. It seems that the use of barite and celestine to increase the mud weight in the VM wells, increased the concentrations of barium and strontium found in the rock.

2.3. Traceable ceramic proppant model

Traceable ceramic proppant, based on kaolinitic clay mixtures with gadolinium and samarium oxides, was modeled in MCNP. An industrial grade, secondary, kaolinitic ball clay was employed as the model clay (APM 112, Piedra Grande-La Toma SA, Neuquén, Argentina) (Herrera et al., 2019; Hernández et al., 2017; Cravero et al., 1997). The chemical composition of the ball clay is shown in Table 4. The analysis was performed by X-Ray Fluorescence Spectrometry, using a Shimadzu Energy Dispersive Spectrometer, model EDX-800HS.

Table 3: Vaca Muerta 5 p.u. water-filled matrix elemental composition used in the simulations. Weight fractions were computed assuming a bulk density of 2.4 g cm^{-3}. Σ = 21.9 c.u., calculated using 1. *Ytterbium cross section data is not available in MCNP5, thus it was not included in the simulations.

Element	Weight fraction (% wt.)	Element	Weight fraction (% wt.)
Oxygen	43.24181447	Lithium	0.00304000
Silicon	20.91756801	Nickel	0.00281200
Calcium	18.09523748	Chromium	0.00243200
Aluminum	5.36290551	Copper	0.00193040
Iron	2.07120590	Lanthanum	0.00189468
Carbon	1.80459599	Yttrium	0.00187036
Potassium	1.80437375	Lead	0.00178220
Sodium	1.31477395	Neodymium	0.00173622
Magnesium	1.20216188	Molybdenum	0.00146722
Sulfur	1.18104000	Thorium	0.00061104
Strontium	1.08885580	Scandium	0.00060420
Hydrogen	0.86237573	Cobalt	0.00058368
Barium	0.37004400	Niobium	0.00045980
Phosphorus	0.22152684	Hafnium	0.00045980
Titanium	0.21298054	Praseodymium	0.00045140
Nitrogen	0.09500000	Cesium	0.00039710
Manganese	0.05822491	Uranium	0.00037042
Vanadium	0.02816566	Samarium	0.00032794
Zinc	0.01919380	Gadolimium	0.00030826
Boron	0.00710600	Dysprosium	0.00029651
Zirconium	0.00684380	Erbium	0.00016078
Rubidium	0.00622136	Ytterbium*	0.00015352
Cerium	0.00362026	Arsenic	0.00001482

Loss on ignition (LOI) was carried out in a muffle furnace at 1,000 ° C for one hour.

Table 4: Chemical composition of the ball clay.

Oxide	Weight fraction (% wt.)	Oxide	Weight fraction (% wt.)
SiO_2	52.709	SO_3	0.061
Al_2O_3	29.733	V_2O_5	0.025
Fe_2O_3	3.704	ZrO_2	0.020
K_2O	1.311	CuO	0.013
TiO_2	0.874	Rb_2O	0.007
MgO	0.791	SrO	0.004
CaO	0.221	Y_2O_3	0.003
Na_2O	0.134		
Loss on ignition	10.390 %		

Different oxide concentrations in the proppant were proposed. The concentration range varied from 0 % to 5 % and 0 % to 10 % by weight of the proppant, in steps by 1 %, for gadolinium and samarium oxides, respectively. From 0 to 1 % a step of 0.1 % was used in both cases.

Ceramic proppant densities were previously determined by our group (Herrera et al., 2019; Hernández et al., 2017) as listed in Table 5. In the simulations, proppants within the range from 0 to 1 % wt. of oxide addition were modeled using ρ_1. While proppants with concentrations higher than 1 % wt., were modeled using ρ_5.

3. Results and discussion

The effect of gadolinium and samarium addition on the detectability of smart proppants was evaluated in limestone and the Vaca Muerta formation, considering a lower and upper hydraulic fracture widths limits of 1 and 10 mm. The

Table 5: Measured densities for clay-Sm_2O_3 and clay-Gd_2O_3 ceramic mixtures.

Content oxide	Density (g cm^{-3})	
	clay-Sm_2O_3	clay-Gd_2O_3
0 % wt. (ρ_0)	2.50	1.98
1 % wt. (ρ_1)	2.11	1.73
5 % wt. (ρ_5)	1.95	1.72

neutron reaction rate was measured in the near, far and extra far detectors (ND, FD and XFD, respectively). The response of the ^{3}He detectors depends, primary, on the distance to the neutron source. Reaction rates are determined by the slowing-down length and thermal neutron diffusion length (Wu et al., 2013; Ellis et al., 2003). Neutron slowing down length is inversely proportional to the slowing down power, determined primary by the hydrogen content of the formation; whereas the thermal neutron diffusion length is inversely proportional to capture cross sections of the individual formation nuclei (Sahay, 2001). The highest reaction rates are recorded in the near detector, while these decrease by several orders of magnitude with increasing source-detector distance.

The neutron reaction rate suppression was calculated in each detector as $(1 - \frac{RR}{RR0}) \times 100\%$, where RR is the computed reaction rate using the traceable compound in the fracture, and $RR0$ is the computed reaction rate without fracture (i.e., before the hydraulic stimulation). From these studies, the minimum concentration of gadolinium and samarium oxides needed, in order to make them detectable by the detectors are determined in each case. Also, it is intended to keep the oxide addition as low as possible provided that the proppant properties are not affected (Liang et al., 2016; Smith et al., 2012; Torres et al., 2012) and its cost is not increased excessively.

3.1. Gadolinium-based proppant detection

The thermal neutron reaction rate measured in the detectors as a function of gadolinium oxide concentration is shown in Figure 2. As shown, the reaction

rate decreases as the concentration increases, following a two-term exponential function. In the Vaca Muerta formation, the reaction rate values determined for all detectors are lower than those measured in the Limestone case (for both fracture widths and gadolinium concentrations). This is related to the presence of thermal absorbers in the formation, such as gadolinium, samarium and boron (See Table 3).

Also, the difference observed between fracture widths (Figure 2), is due to the presence of the highest amount of gadolinium in the fracture of 10 mm width, giving the lowest reaction rate measurements.

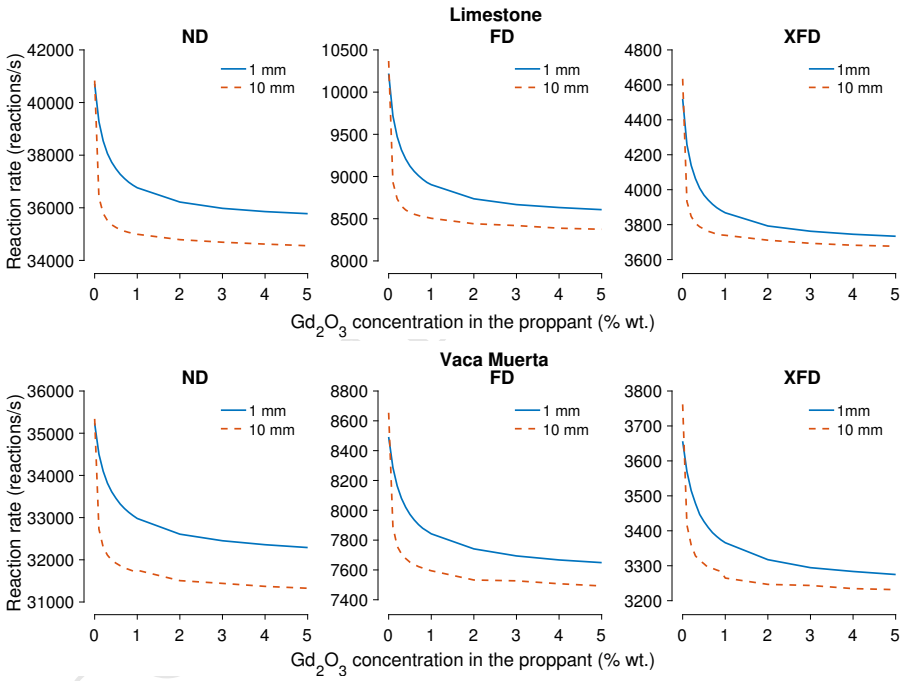

Figure 2: Neutron reaction rate measured in the near, far and extra far detectors (ND, FD and XFD, respectively) as a function of gadolinium oxide concentration in Limestone of 20 p.u. water-filled (top) and the Vaca Muerta formation of 5 p.u. water-filled (bottom). Two fractures widths were assumed.

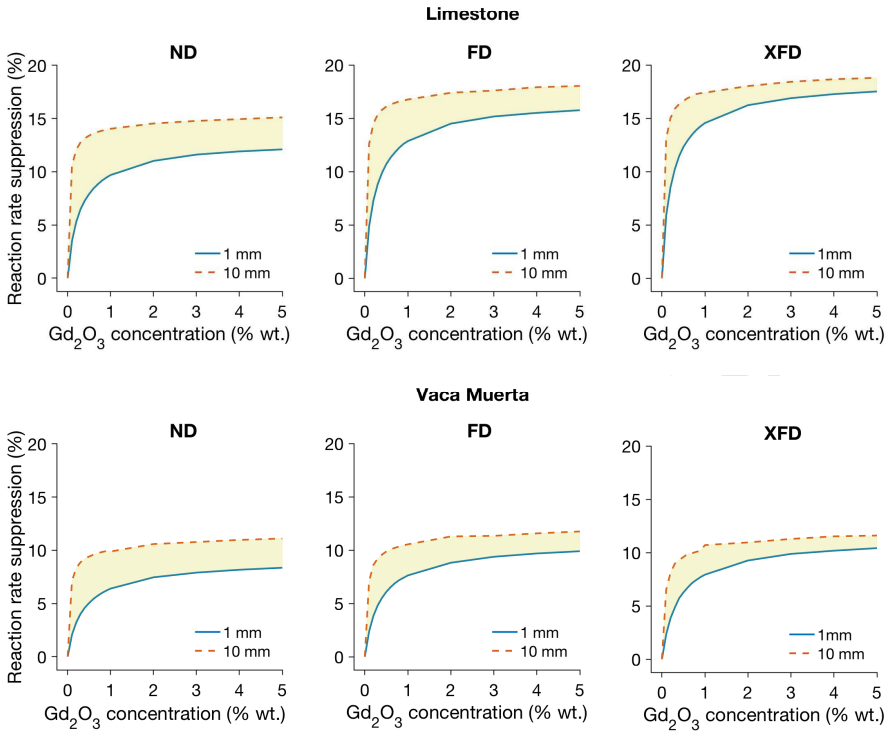

Figure 3: Neutron reaction rate suppression computed in the Near, Far and Extra Far detectors (ND, FD and XFD, respectively) as a function of gadolinium oxide concentration, in Limestone (upper) and the Vaca Muerta (bottom) formation model.

3.1.1. Gadolinium oxide concentration

Figure 3 depicts the neutron reaction rate suppression due to the gadolinium oxide addition from 0 to 5 % by weight of the proppant, in the reference case of study and in the Vaca Muerta formation model. The 0 % data refers to a pure ceramic proppant (i.e., without traceable material). As can be seen in the figures, there is a significant rise in the reaction rate suppression from 0 to 1 % wt. addition in the proppant. After this value, the fractional loss increases slowly for each detector. In particular, the reaction rate suppression was not affected significantly by the detector position in the Vaca Muerta case. Gadolinium oxide additions higher than 1 % by weight of the proppant, contributed with an increase of 2 % in the fractional loss, at the most. A saturation effect can be seen

in both formations and fracture widths (Figure 3). As expected, the neutron suppression is increased in the widest fracture case due to the higher amount of absorbing material near wellbore (i.e., more captures are produced). However, the thinnest fracture width of 1 mm is actually, nearly the one produced by the hydraulic fracturing process in Vaca Muerta (Ortiz et al., 2016).

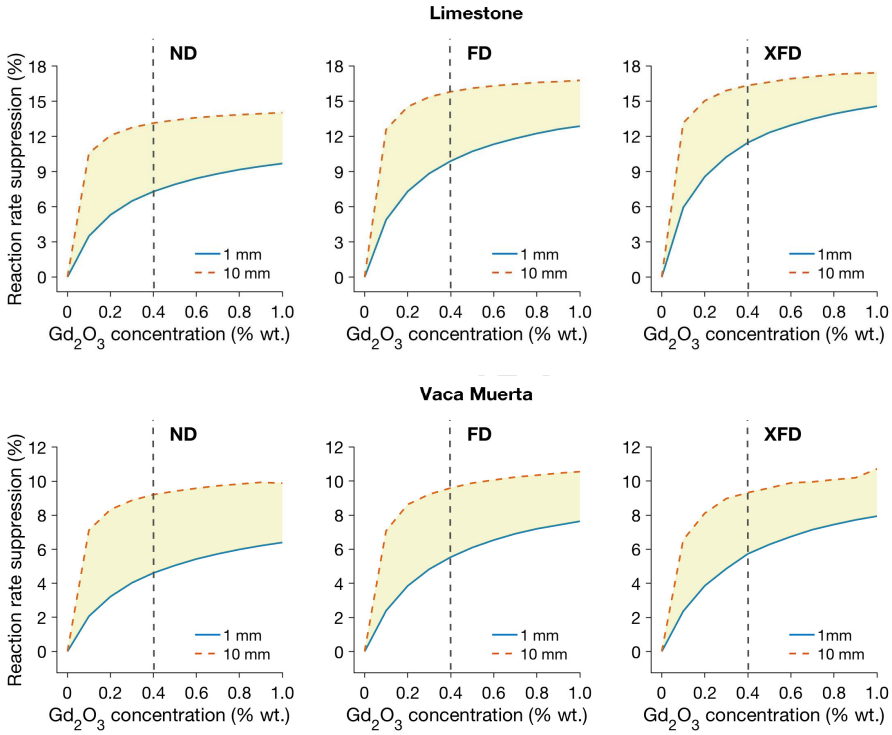

Figure 4: Detail of the reaction rate suppression curves from 0 to 1 % wt. of gadolinium oxide concentration in the ceramic proppant. Vertical dashed line indicates the Gd_2O_3 concentration used in a commercial proppant (Torres et al., 2012).

The results are in agreement with previous reported values under similar conditions in a limestone formation (Zhang and Smith, 2017; Liu et al., 2015; Smith et al., 2013). The addition of gadolinium oxide into a bauxitic ceramic proppant was previously determined to be in a range from 0.025 % to 1 % by weight of the proppant (Smith et al., 2012). Moreover, the commercial ceramic proppant

CarboNRT®, uses 0.4 % by weight of gadolinium oxide addition (Zhang and Smith, 2017; Smith et al., 2013; Torres et al., 2012). This value is indicated by a vertical dashed line in Figure 4, where a detail of the reaction rate suppression curves from 0 to 1 % by weight of gadolinium oxide concentration is shown. The addition of 0.4 % by weight of the proppant produced a reaction rate suppression in the near detector of 7.3 and 4.6 % in the Limestone and Vaca Muerta formations, respectively, for a fracture width of 1 mm. Higher suppressions are achieved in far and extra far detectors (See Table 6).

A difference of proximately −6 % in the reaction rate suppression is reached between fracture widths (Figure 4), when using a 0.4 % of gadolinium oxide addition in Limestone, for ND and FD. In the case of XFD, the difference is −4.8 %. These values represent a significant decrease (of about 44, 37 and 29 % for ND, FD and XFD, respectively) in the reaction rate suppression between fracture widths.

In the case of Vaca Muerta, a difference of −4.6, −4.1 and −3.6 % in the reaction rate suppression is reached between fracture widths (Figure 4) for ND, FD and XFD, respectively. These represent a decrease of 50, 43 and 39 %, respectively, in the suppression between fracture widths.

The reaction rate suppression values are significantly different between the reference case of study and the realistic condition. Figure 5 shows the comparison between Limestone and Vaca Muerta formations in terms of the reaction rate suppression obtained in the detectors. The sensitivity loss of the measurements in the Vaca Muerta formation can be appreciated, with reaction rate suppressions decreasing between 2 to 8 % (for different additions), compared to Limestone.

3.2. Samarium-based proppant detection

Figure 6 is similar to Figure 2, replacing gadolinium by samarium. Neutron reaction rates measured in the near, far and extra far detectors showed similar behavior to those found in curves with gadolinium (Figure 2). These curves de-

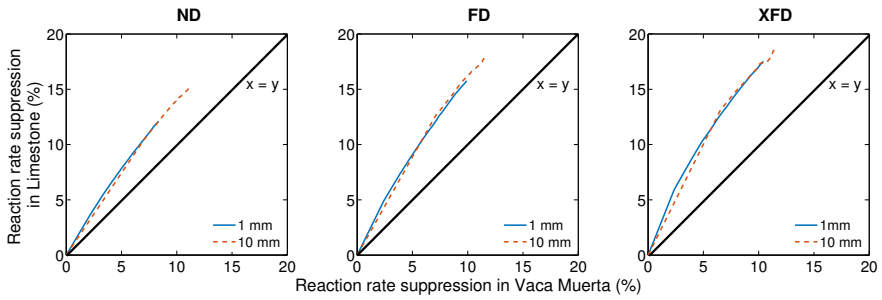

Figure 5: Neutron reaction rate suppression computed in the Near, Far and Extra Far detectors (ND, FD and XFD, respectively) in Limestone compared to the reaction rate suppression in Vaca Muerta. The straight line $x = y$ indicates equal percentage of suppression.

crease as the concentration increases, following a two-term exponential function. As it is expected, the suppression rate is slower than that of the gadolinium's, due to the macroscopic capture cross sections between materials (9.3 c.u. and 21.9 c.u. for limestone and Vaca Muerta, respectively).

When samarium is used, approximately 3 and 1.5 times of gadolinium oxide addition is needed to obtain the same number of reactions per second in the detectors, for 1 and 10 mm fracture widths, respectively.

3.2.1. Samarium oxide concentration

Figure 7 depicts the neutron reaction rate suppression due to Sm_2O_3 addition from 0 to 10 % by weight of the proppant, in the reference case of study and in the Vaca Muerta formation model. The 0 % data refers to a pure ceramic proppant (i.e., without traceable material). As in the gadolinium's case, there is a rise in the reaction rate suppression from 0 to 3 % wt. addition in the proppant. After this value, the fractional loss increases slowly for each detector. In particular, after this concentration value, the reaction rate suppression increases only of about 2 and 1 % in Limestone, for 1 and 10 mm fracture widths, respectively. The same occurs in the Vaca Muerta formation.

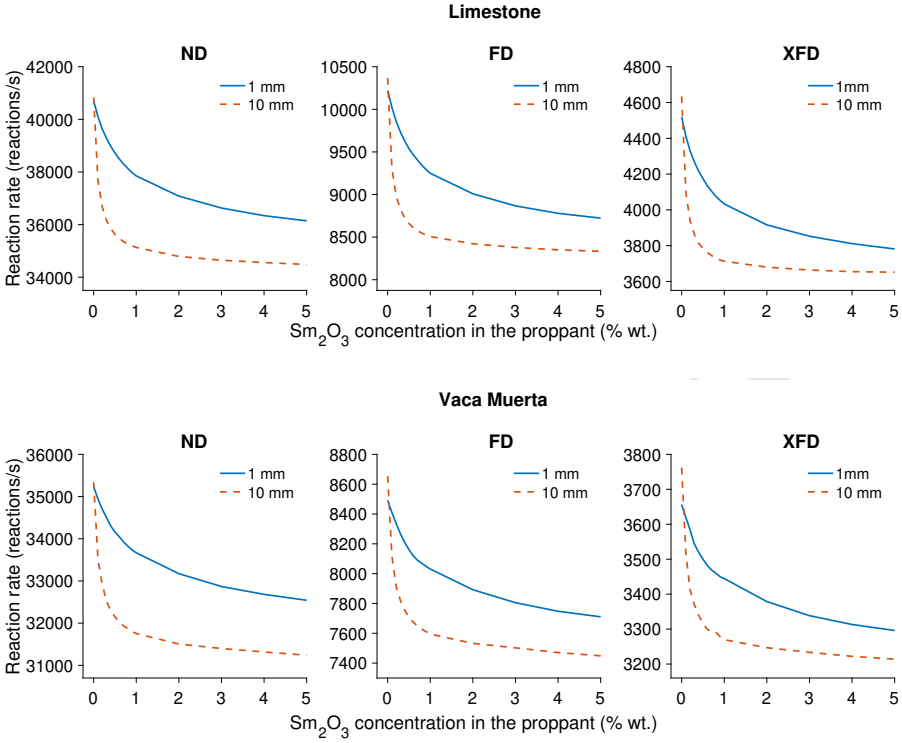

Figure 6: Neutron reaction rate measured in the near, far and extra far detectors (ND, FD and XFD, respectively) as a function of samarium oxide concentration in Limestone of 20 p.u. water-filled (top) and the Vaca Muerta formation of 5 p.u. water-filled (bottom). Two different fractures width were assumed.

A detail of the reaction rate suppression curves from 0 to 3 % wt. of samarium oxide concentration in the ceramic proppant is shown in Figure 8. As it is shown, the curves are approached an asymptotic limit in the Limestone and Vaca Muerta formation cases, for concentrations higher than 1 % wt. of samarium oxide and 10 mm fracture width. However, this approach is not observable in the thinnest fracture. Both Limestone and Vaca Muerta formations show a rise without an asymptotic tendency from 0 to 3 %. In this range, concentrations higher than 2 % an produced an increase in the signal of only 1 % in all cases.

Since in the present case there is no asymptotic limit, the "optimum" oxide

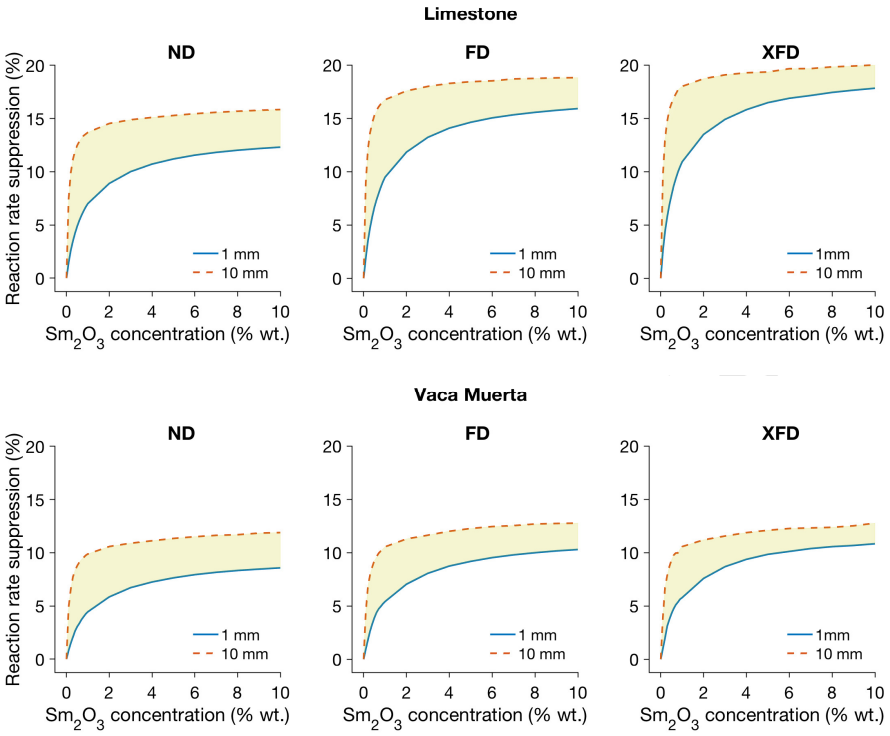

Figure 7: Neutron reaction rate suppression computed in the Near, Far and Extra Far detectors (ND, FD and XFD, respectively) as a function of samarium oxide concentration, in Limestone (upper) and the Vaca Muerta formation model (bottom).

concentration is not evident. Thus, a minimum samarium oxide addition was chosen to produce the same reaction rate suppression obtained in the gadolinium's case, using 0.4 % wt. of gadolinium oxide addition in Limestone and 1 mm fracture width (i.e., the most conservative case). As it is shown in Table 6, the reaction rate suppression value of 7.3 % in the near detector implies 1.25 % by weight of samarium oxide addition in the proppant.

Using a concentration of 1.25 % by weight of Sm_2O_3 in Vaca Muerta, will produce a reaction rate suppression in the near detector of 7.3 and 4.6 % in the Limestone and Vaca Muerta formations, respectively, for a fracture width of 1 mm. Higher suppressions are achieved in far and extra far detectors (See Table

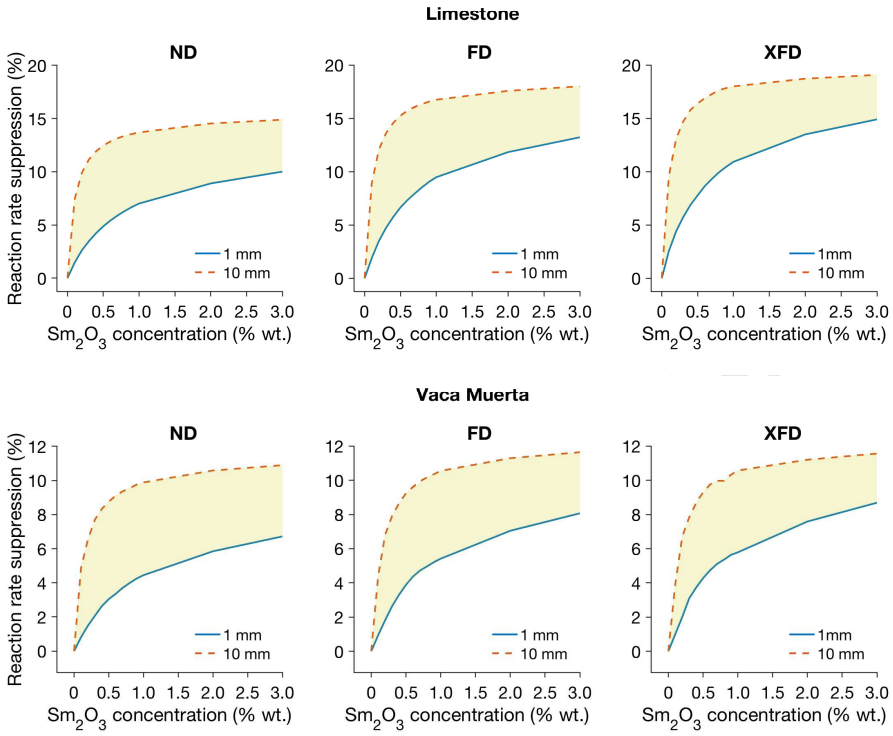

Figure 8: Detail of the reaction rate suppression curves from 0 to 1 % wt. of samarium oxide concentration in the ceramic proppant. Vertical dashed line indicates the Gd_2O_3 concentration used in a commercial proppant (Torres et al., 2012).

6).

A difference of proximately −7 % in the reaction rate suppression is reached between fracture widths (Figure 8) when using a 1.25 % of samarium oxide addition in Limestone, for ND and FD. In the case of XFD, the difference is −6.2 %. These values represent a significant decrease (of about 48, 40 and 33 % for ND, FD and XFD, respectively) in the reaction rate suppression between fractures widths.

In the case of Vaca Muerta, a difference of −5.4, −3.9 and −4.6 % in the reaction rate suppression is reached between fracture widths (Figure 8) for ND, FD and XFD, respectively. These represent a decrease of 54, 36 and 43 %, respectively, in the suppression between fracture widths.

Table 6: Reaction rate suppression obtained in the near, far and extra far detectors (ND, FD, XFD, respectively), using minimum gadolinium and samarium oxides concentrations in Limestone and Vaca Muerta formations with 1 and 10 mm fracture widths.

Formation	Width (mm)	Oxide	Addition (% wt.)	Suppression (%)		
				ND	FD	XFD
Limestone	1	Gd_2O_3	0.4	**7.3**	9.9	11.5
20 p.u.	10	Gd_2O_3	0.4	13.1	15.8	16.3
	1	Sm_2O_3	1.25	**7.3**	10.0	12.0
	10	Sm_2O_3	1.25	14.0	16.8	18.0
Vaca Muerta	1	Gd_2O_3	0.4	4.6	5.5	5.7
5 p.u.	10	Gd_2O_3	0.4	9.2	9.6	9.3
	1	Sm_2O_3	1.25	4.6	6.9	6.2
	10	Sm_2O_3	1.25	10.0	10.8	10.8

The comparison between the results in Limestone and Vaca Muerta, are shown in Figure 9. The reaction rate suppression values are significantly different from the reference case of study and a realistic condition. Compared to Limestone, a sensitivity loss in the Vaca Muerta measurements can be appreciated, with reaction rate suppressions decreasing between 1 to 4 %, for different additions.

4. Conclusion

In this work a borehole-formation-tool system was modeled with MCNP. The Vaca Muerta formation was described in MCNP, based on measured geochemical data. Ceramic proppant traced with gadolinium and samarium oxides were also modeled based on experimental data of a clay-Gd_2O_3 and clay-Sm_2O_3 materials.

In the case of gadolinium, the results are in agreement with previous reported

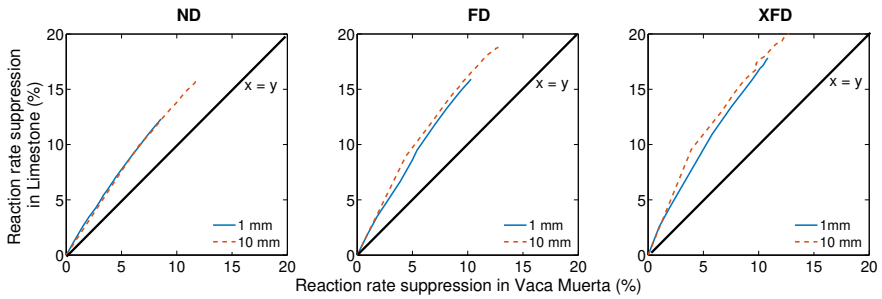

Figure 9: Neutron reaction rate suppression computed in the Near, Far and Extra Far detectors (ND, FD and XFD, respectively) in Limestone compare to the reaction rate suppression in Vaca Muerta. The straight line $x = y$ indicates equal suppression percentages.

gadolinium oxide concentrations in a range from 0.025 % to 1 % by weight of proppant (Smith et al., 2012; Torres et al., 2012) in a Limestone formation of 20 p.u. water-filled. A minimum gadolinium oxide concentration of 0.4 % by weight could be detected in the Vaca Muerta formation.

In the case of samarium, to be detected, a minimum concentration of samarium oxide of 1.25 % by weight is required in both Limestone and Vaca Muerta formations.

It was previously shown by our group, that the thermo-chemical complex processes of the ceramic material are not affected by the presence of such samarium oxide concentration (Herrera et al., 2019). This fact, together with the present results shows the possibility of using samarium oxide as an alternative to gadolinium oxide in traceable smart proppants.

Acknowledgment

This work has been partially supported by Nano-Petro FONARSEC Project 2012 (ANPCyT) and ANPCyT grant PICT-2016-0463. MSH wants to express her gratitude to Dr. Manuel Sztejnberg for MCNP technical exchanges. The authors wish to thank YPF S.A. and YPF Tecnología S.A. for permission to

publish this paper.

References

Amaro, F.D., Monteiro, C.M.B., dos Santos, J.M.F., Antognini, A., 2017. Novel concept for neutron detection: proportional counter filled with ^{10}B nanoparticle aerosol. Scientific Reports 7, 1–6. doi:http://doi.org/10.1038/srep41699.

Cravero, F., González, I., Galán, E., Dominguez, E., 1997. Geology, mineralogy, origin and possible applications of some argentinian kaolins in the Neuquén basin. Applied Clay Science 12, 27–42. doi:10.1016/S0169-1317(96)00035-X.

Duenckel, R.J., Palisch, T.T., Han, X., Saldungaray, P., 2014. Environmental stewardship: Global applications of a nonradioactive method to identify proppant placement and propped-fracture height. SPE Production & Operations 29, 231–242. doi:https://doi.org/10.2118/166251-PA.

Duenckel, R.J., Smith, H., Warren, W.A., Grae, A.D., 2011. Field application of a new proppant detection technology. SPE 93, 28–35.

EIA, 2013. Technically Recoverable Shale oil and Shale Gas Resources: An Assessment of 137 Shale Formations in 41 Countries Outside the United States. Technical Report SAND2014-17693. EIA, Energy Information Administration. Department of Energy, Washington DC. URL: http://www.eia.gov/analysis/studies/worldshalegas/pdf/overview.pdf.

Ellis, D.V., Case, C.R., Chiaramonte, J.M., 2003. Tutorial - Porosity from Neutron Logs I - Measurement. Petrophysics 44, 383–395.

Forster, R.A., Little, R.C., Briesmeister, J.F., Rendricks, J.S., 1990. MCNP capabilities for nuclear well logging calculations. IEEE Transactions on nuclear science 37, 1378–1385.

Han, X., Duenckel, R., Smith, H., Smith, H.D., 2014. An Environmentally Friendly Method to Evaluate Gravel and Frac Packed Intervals Using a New Non-Radioactive Tracer Technology. In: Offshore Technology Conference, Houston, USA, 05-08 May. doi:10.4043/25166-MS.

Hernández, M.F., Conconi, M.S., Cipollone, M., Herrera, M.S., Rendtorff, N.M., 2017. Ceramic behavior of ball clay with gadolinium oxide (Gd2O3) addition. Applied Clay Science 146, 380–387. URL: http://www.sciencedirect.com/science/article/pii/S0169131717302818, doi:https://doi.org/10.1016/j.clay.2017.06.021.

Herrera, M.S., Hernández, M.F., Cipollone, M., Conconi, M.S., Rendtorff, N.M., 2019. Thermal behavior of samarium oxide - Ball clay mixtures for high macroscopic neutron capture cross section ceramic materials. Applied Clay Science 168, 125–135. URL: http://www.sciencedirect.com/science/article/pii/S0169131718304496, doi:https://doi.org/10.1016/j.clay.2018.10.010.

Liang, F., Sayed, M., Al-Muntasheri, G.A., Chang, F.F., Li, L., 2016. A comprehensive review on proppant technologies. Petroleum 2, 26 – 39. URL: http://www.sciencedirect.com/science/article/pii/S2405656115000693, doi:https://doi.org/10.1016/j.petlm.2015.11.001.

Liu, J., Zhang, F., Gardner, R.P., Hou, G., Zhang, Q., Li, H., 2015. A method to evaluate hydraulic fracture using proppant detection. Applied Radiation and Isotopes 105, 139–143. URL: http://www.sciencedirect.com/science/article/pii/S0969804315301433, doi:https://doi.org/10.1016/j.apradiso.2015.08.003.

Maucec, M., Spanier, J., 2000. The MCNP perturbation feature assessment for nuclear logging Monte Carlo calculations. In: International Conference Nuclear Energy in Central Europe 2000, Slovenia, 11-14 September.

McConn, R.J., Gesh, C.J., Pagh, R.T., Rucker, R.A., Williams III, R., 2011. Compendium of Material Composition Data for Radiation Transport Modeling. Technical Report PNNL-15870 Rev. 1. Pacific Northwest National Laboratory, Richland, WA. URL: http://www.pnl.gov/publications/abstracts.asp?report=359067.

Mendoza, A., Preeg, W.E., Torres-Verdín, C., Alpak, F.O., 2007. Monte Carlo modeling of nuclear measurements in vertical and horizontal wells in the presence of mud-filtrate invasion and salt mixing. Petrophysics 48, 28–44.

Mocciaro, A., Lombardi, M.B., Scian, A.N., 2018. Effect of raw material milling on ceramic proppants properties. Applied Clay Science 153, 90 – 94. URL: http://www.sciencedirect.com/science/article/pii/S0169131717305586, doi:https://doi.org/10.1016/j.clay.2017.12.009.

Oliveria Neto, J.M., Yakovlev, A., 2017. The use of pre & post fracture stimulation logs to better integrate static petrophysical analysis with dynamic data from production logs. In: SPWLA 59th Annual Logging Symposium, London, UK, 2-6 June.

Ortega, E., Torres-Verdín, C., Preeg, W.E., 2014. Rapid forward modeling of multidetector logging-while-drilling sigma measurements. Geophysics 79, D253–D273. doi:10.1190/geo2014-0031.1.

Ortiz, A.C., Hryb, D.E., Martínez, J.R., Varela, R.A., 2016. Hydraulic Fracture Height Estimation in an Unconventional Vertical Well in the Vaca Muerta Formation, Neuquén Basin, Argentina. In: SPE Hydraulic Fracturing Technology Conference, The Woodlands, Texas, USA, 9-11 February.

Preeg, W.E., Scott, H.D., 1986. Computing thermal neutron decay time environmental effects using Monte Carlo techniques. SPE Formation Evaluation 1, 35–42.

Russell DePriest, K., Saavedra, K.C., 2014. MatMCNP: A Code for Producing Material Cards for MCNP. Technical Report SAND2014-17693. Sandia

National Laboratories, Albuquerque, New Mexico 87185 and Livermore, California 94550. URL: http://www.pnl.gov/publications/abstracts.asp?report=359067.

Sagasti, G., Ortiz, A., Hryb, D., Foster, M., Lazzari, V., 2014. Understanding Geological Heterogeneity to Customize Field Development: An Example From the Vaca Muerta Unconventional Play, Argentina. In: SPE/AAPG/SEG Unconventional Resources Technology Conference, Denver, Colorado, USA, 25-27 August.

Sahay, B., 2001. Petroleum Exploration and Exploitation Practices. 3 ed., Allied Publishers Pvt. Ltd., New Dheli.

Saldungaray, P., Duenckel, R.J., Palisch, T.T., 2014. Reducing Hydraulic Fracturing HSE Footprint through the Application of a Non-Radioactive Method for Proppant Placement and Propped Fracture Height Assessment. In: SPE Middle East Health, Safety, Environment & Sustainable Development Conference and Exhibition, Doha, Qatar, 22-24 September.

Serov, I.V., John, T.M., Hoogenboom, J.E., 1998. A new effective monte carlo midway coupling method in MCNP applied to a well logging problem. Applied Radiation and Isotopes 49, 1737 – 1744. URL: http://www.sciencedirect.com/science/article/pii/S0969804398000554, doi:https://doi.org/10.1016/S0969-8043(98)00055-4.

Smith, H., Duenckel, R., 2014. Spectral identification of proppant in subterranean fracture zones. URL: https://www.google.ch/patents/US8648309. US Patent 8,648,309.

Smith, H., Smith, M., Duenckel, R., 2012. Methods of identifying high neutron capture cross section doped proppant in induced subterranean formation fractures. URL: https://www.google.ch/patents/US8234072. US Patent 8,234,072.

Smith, H.D., Duenckel, R., Han, X., 2013. A new nuclear logging method to locate proppant placement in induced fractures. Petrophysics 54, 415–426.

Stinco, L., Barredo, S., 2014. Vaca Muerta Formation: An Example of Shale Heterogeneities Controlling Hydrocarbon's Accumulations. In: SPE/AAPG/SEG Unconventional Resources Technology Conference, Denver, Colorado, USA, 25-27 August.

Suarez, M., s. Pichon, Lacentre, P., Fernandez Badessich, M., 2015. Fracturing-to-Production Simulation Approach for Completion Optimization in the Vaca Muerta Shale. In: SPE Latin American and Caribbean Petroleum Engineering Conference, Quito, Ecuador, 18-20 November.

Suarez, M., Vega Velasquez, L., Monti, L.J., Thompson, A.R., 2013. Modeling Vertical Multifractured Wells in Vaca Muerta Shale Oil Play, Argentina. In: SPE Unconventional Resources Conference-USA, The Woodlands, Texas, USA, 10-12 April.

Torres, F., Reinoso, W., Chapman, M., Han, X., Campo, P., 2012. Field application of new proppant-detection technology - A case history in the Putumano basin of Colombia. In: SPE Latin America and Caribbean Petroleum Engineering Conference, Mexico City, Mexico, 16-18 April.

van der Hoeven, C., Montgomery, M., Sablan, G., Schneider, E., Torres-Verdín, C., 2017. Gadolinium tracers for enhancement of sigma-log contrast measurements. Geophysics 82, EN13–EN24. doi:https://doi.org/10.1190/geo2016-0195.1.

Wang, S., Xiao, L., Yue, A., Wang, H., Liu, W., Fan, Y., 2017. Accurate inversion of elemental concentrations from the pulsed neutron geochemical logging based on an active-set method. Journal of Petroleum Science and Engineering 157, 833 – 841. URL: http://www.sciencedirect.com/science/article/pii/S0920410517306253, doi:https://doi.org/10.1016/j.petrol.2017.07.075.

Wielopolski, L., Song, Z., Orion, I., Hanson, A.L., Hendrey, G., 2005. Basic considerations for Monte Carlo calculations in soil. Applied Radiation and Isotopes 62, 97–107. URL: http://www.sciencedirect.com/science/article/pii/S096980430400394X, doi:https://doi.org/10.1016/j.apradiso.2004.06.003.

Wu, W., Tong, M., Xiao, L., Wang, J., 2013. Porosity sensitivity study of the compensated neutron logging tool. Journal of Petroleum Science and Engineering 108, 10–13.

X-5 Monte Carlo Team, 2008. MCNP – A General Monte Carlo N-Particle Transport Code, Version 5. Technical Report LA-UR-03-1987. Los Alamos National Laboratory.

Zhang, J., Smith, H.D., 2017. A Determination of the Capability of Using Gadolinium Tagged Proppant To Evaluate Propped Fracture Width. In: SPWLA 58th Annual Logging Symposium, Oklahoma City, Oklahoma, USA, 17-21 June.

Zhang, J., Smith, H.D., Palisch, T., 2018. A Novel Technology for Locating and Evaluating Hydraulic Fractures in Horizontal Wells Modeling and Field Results. In: SPE Annual Technical Conference and Exhibition, Dallas, USA, 24-26 September. doi:https://doi.org/10.2118/191707-MSS.